https://doi.org/10.5194/egusphere-2026-3447
Preprint. Discussion started: 29 June 2026

Does the envelope of Rossby wave packets exhibit higher predictability than the underlying wave pattern?

Michael Riemer[1] and Lorenz Gölz[1]

[1]Institut für Physik der Atmosphäre, Johannes Gutenberg-Universität, Mainz, Germany

Correspondence: Michael Riemer (mriemer@uni-mainz.de)

Abstract. This study tests the long-standing hypothesis that Rossby wave packet (RWP) envelopes exhibit enhanced predictability compared to embedded weather systems, here interpreted as the individual troughs and ridges comprising the underlying wave pattern. Using a potential vorticity framework and the saturation fraction of the mean square error as a predictability metric, we derive a tendency equation for envelope errors to diagnose error-growth mechanisms. Contrary to the hypothesis, our analysis does not reveal any evidence of enhanced envelope predictability. The error dynamics of the envelope and the underlying wave pattern are strikingly similar. Crucially, while the envelope discards information about the location of troughs and ridges (phase information), it remains sensitive to the relative phase relationships among constituent wavenumbers. Phase errors in the individual wavenumbers may directly propagate into envelope errors, demonstrating that "the envelope is the wave", i.e, the dynamics of the envelope are intrinsically governed by its underlying wavenumbers, not by larger-scale dynamics. At least up to lead times of 10 days, the longest lead times considered herein, envelope predictability is thus governed by the same dynamical constraints as the synoptic-scale Rossby wave field. The misconception of RWPs as a larger-scale, dynamical phenomenon may arise by noting the continent- or ocean-basin-wide scale of RWP ”objects” on spatial maps. Confirming previous work, we find enhanced predictability in the presence of RWPs compared to situations without RWPs. This enhanced predictability arises because RWPs organize high-amplitude anomalies coherently over large scales – not from the envelope itself. The spatial coherence of high-amplitude anomalies within RWPs is arguably facilitated by a strong midlatitude waveguide, suggesting waveguide characteristics as a promising target for future predictability research.

1 Introduction

Rossby wave packets (RWPs) organize large-scale energy transport in the atmosphere. The significance of this energy transport for atmospheric predictability and teleconnections has long been recognized (Namias and Clapp, 1944; Cressman, 1948; Grose and Hoskins, 1979). Here we focus on RWPs along the midlatitude jet (Wirth et al., 2018), which have more recently received attention as potentially predictable precursors to high-impact weather events (e.g. Shapiro and Thorpe, 2004; Grazzini, 2007; Martius et al., 2008; Piaget et al., 2015; Fragkoulidis et al., 2018; Grazzini et al., 2021). RWPs are often considered as physical entities with spatio-temporal scales larger than those of the associated individual troughs and ridges. This perspective leads to the notion that RWPs are a phenomenon on scales larger than the synoptic scale.

https://doi.org/10.5194/egusphere-2026-3447
Preprint. Discussion started: 29 June 2026

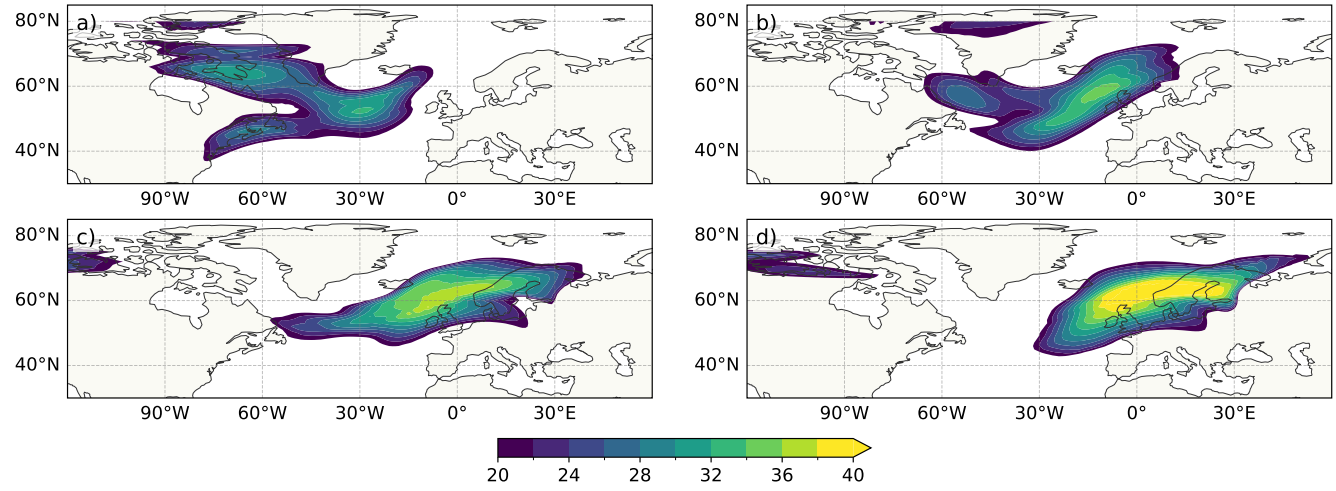

Figure 1. Illustration of the envelope (in m s^{-1}) of an RWP in the North Atlantic – European region, computed using the refined method by Wolf and Wirth (2017), for August 6–9 at 12 UTC (a) - d)). The case is taken from Fragkoulidis et al. (2018).

Considering RWPs as physical entities underlies the often used practice to identify and track RWPs as coherent regions in which the Rossby-wave envelope exceeds a certain threshold (e.g. Zimin et al., 2003; Souders et al., 2014; Grazzini and Vitart, 2015; Wolf and Wirth, 2017, see Fig. 1 for illustration). The envelope is constructed by spectral filtering, retaining waves only within a wavenumber range that represents midlatitude, baroclinic Rossby waves, e.g., (zonal) wavenumbers 4–15. Hereafter, we will refer to the superposition of the waves within this wavenumber range as the underlying wave pattern. The envelope describes spatial variations of wave amplitude but eliminates information about the location of individual troughs and ridges, i.e., phase information. A formal definition of the envelope will be given below. The envelope perspective has led to the hypothesis that "the packet envelope should be more predictable than the individual weather systems", "[b]ecause the packet can remain coherent despite chaotic internal dynamics" (Lee and Held, 1993, their pg. 1428).

To our knowledge, the hypothesis by Lee and Held (1993) has not yet been explicitly tested. Testing this hypothesis is a primary goal of this study. For our test, we interpret Lee and Held's "individual weather systems" as the troughs and ridges that compose the underlying wave pattern. The hypothesis of increased predictability of the RWP envelope is plausible because there are two potential sources of increased predictability. First, the envelope identifies RWPs as physical entities that are larger-scale features than individual troughs and ridges (as indicated in Fig. 1). Due to the well-known scale dependence of predictability (Lorenz, 1969), a larger-scale feature can be expected in general to exhibit higher predictability. Second, the envelope eliminates information about the phase of individual troughs and ridges. Studies investigating error decomposition (Jankov et al., 2021) and lead-time dependence of error-growth mechanisms (Baumgart et al., 2018; Baumgart and Riemer, 2019) indicate that early error growth is associated with phase rather than with amplitude errors. Removing phase information can be expected to reduce errors and may thereby increase predictability.

https://doi.org/10.5194/egusphere-2026-3447
Preprint. Discussion started: 29 June 2026

We use ERA5 re-forecast data verified against ERA5 re-analysis to compare the predictability of RWP envelopes and the underlying wave pattern. The re-forecasts provide lead times up to 10 days, i.e, we consider medium-range predictability. For fair comparison, we apply the same forecast metric to both the RWP envelope and the underlying wave pattern, namely the mean-squared error (MSE). Previous studies have evaluated RWP envelopes in forecasts using object-based (Quinting and Vitart, 2019; Pérez-Fernández and Barreiro, 2023) or field-deformation methods (Prestel-Kupferer et al., 2024) to avoid the well-known double-penalty issue when verifying coherent features using MSE-type metrics (Ebert and McBride, 2000; Baldwin and Kain, 2006). It is not clear to us, however, how a comparable object-based method could be designed for the underlying wave pattern. While a field-deformation method could be applied to the wave pattern, to our knowledge, these methods do not provide a theoretical value of the error saturation level. Considering errors relative to their saturation level, however, is common practice in studies of intrinsic predictability, going back at least to Lorenz (1969, his Fig. 2). Normalizing errors of different phenomena by their respective saturation levels is crucial for a fair comparison of predictability. This important point will further be illustrated at the beginning of Sect. 4, before presenting our actual results. Arguably, such a normalization effectively negates the double-penalty issue. We thus consider the MSE, for which the saturation level is well known, as an appropriate metric for the purpose of this study.

We seek further understanding of predictability characteristics by investigating the underlying error-growth mechanisms. As noted above, it is plausible to expect that errors of the RWP envelope signifies amplitude errors of the underlying wave pattern. Errors of the envelope may thus be expected to grow by mechanisms that impact wave amplitude, whereas errors of the underlying wave pattern grow in addition by mechanisms that impact wave phase. To examine error-growth mechanisms, we employ a potential-vorticity (PV) framework first introduced by Davies and Didone (2013) to study the dynamics of forecast errors and subsequently extended to piecewise PV thinking (Hoskins et al., 1985) by Baumgart et al. (2018); Baumgart and Riemer (2019). This framework provides a tendency equation for PV errors near the tropopause, which is applicable to RWPs because RWP dynamics can be succinctly described by near-tropopause, piecewise PV tendencies (Teubler and Riemer, 2016, 2021). The existing framework is directly applicable to errors of the underlying wave pattern using respective spectral filtering of error tendencies. The extension of the framework to envelope errors will be presented in Sect. 3, along with a dynamical interpretation of the individual tendency terms. Whereas RWPs are more commonly studied using upper-tropospheric winds, our interest in understanding predictability from the perspective of the governing error-growth mechanisms motivates the use of PV as the main variable in this study.

The next section describes established types of data and methods employed in this study, including a catalog of objectively identified RWP objects, the computation of the (PV) envelope field, and how to determine appropriate saturation levels. Section 3 introduces the piecewise PV-tendency framework. Based on results presented in Sect. 4.1, the hypothesis by Lee and Held (1993) will need to be rejected. Dynamical insight in this result is discussed in Sect. 4.2. The general notion that the very presence of RWPs increases predictability (Grazzini and Vitart, 2015) is revisited in Sect. 4.3. Finally, Sect. 5 provides a summary and concluding discussion.

https://doi.org/10.5194/egusphere-2026-3447
Preprint. Discussion started: 29 June 2026

2 Data and methods

2.1 Data

2.1.1 ERA5 re-forecasts

The primary data set for this study are ERA5 re-forecasts, which have been produced at the European center of medium-range weather forecasts (ECMWF) retrospectively using the ERA5 model (Hersbach et al., 2020) and ERA5 reanalysis as initial conditions. Accordingly, we verify these re-forecasts against ERA5 reanalysis. The ERA5 model is version Cy41r2 of the Integrated Forecasting System, which was operational at ECMWF from March 8 – November 22, 2016. We here use forecasts initialized daily at 0000 and 1200 UTC from January 2000 – December 2018. Re-forecasts are available to us at 12-hourly lead times up to +240 h on a regular latitude–longitude grid of $1^\circ \times 1^\circ$ horizontal resolution and on 17 pressure levels (1000, 950, 925, 900, 850, 800, 700, 600, 500, 400, 300, 250, 200, 150, 100, 70, and 50 hPa).

2.1.2 Catalog of Rossby wave packets

We use a catalog of RWP occurrence previously compiled by Prestel-Kupferer et al. (2024). The RWPs in this catalog were identified and tracked as RWP-objects using 3-hourly ERA5 reanalysis data for the years 2000–2018. Following Wolf and Wirth (2017), RWP-objects are defined based on the envelope of the 300-hPa wind component that is perpendicular to the streamlines of a background flow (as in Zimin et al., 2006). Asymmetries in the along-flow scale of troughs and ridges are reduced by the semi-geostrophic transformation suggested by Wolf and Wirth (2015). The specific procedure is described in detail in Sect. 2.2 in Prestel-Kupferer et al. (2024), along with a comparison of the resulting RWP sample with previously published RWP climatologies. In general, there is a large degree of consistency with previous results. A specific difference between the Prestel-Kupferer et al. sample and that of Grazzini and Vitart (2015) occurs in the monthly variation of total RWP numbers, with less winter than summer cases (in relative terms) in the Prestel-Kupferer et al. sample. This difference implies a potential bias of year-round averages towards summer cases. The results of this study are not affected by such a potential bias, because we find qualitative agreement when considering summer and winter seasons individually.

Following previous studies, we consider RWP-objects with a life time of 3–14 days, resulting here in a sample of 1147 RWPs. The occurrence frequency of the RWP-objects considered herein is illustrated for the extended winter and extended summer seasons (defined as the months November–March and May–September, respectively) in Fig. 2a,b. The occurrence frequency maximizes in the maritime storm tracks, but RWPs traverse the continental regions also, in particular North America. The current study uses RWP-objects merely to restrict the verification of field-based metrics to the region of RWP-objects. We therefore do not expect sensitivity of our results to the precise definition and selection of RWP-objects.

https://doi.org/10.5194/egusphere-2026-3447
Preprint. Discussion started: 29 June 2026

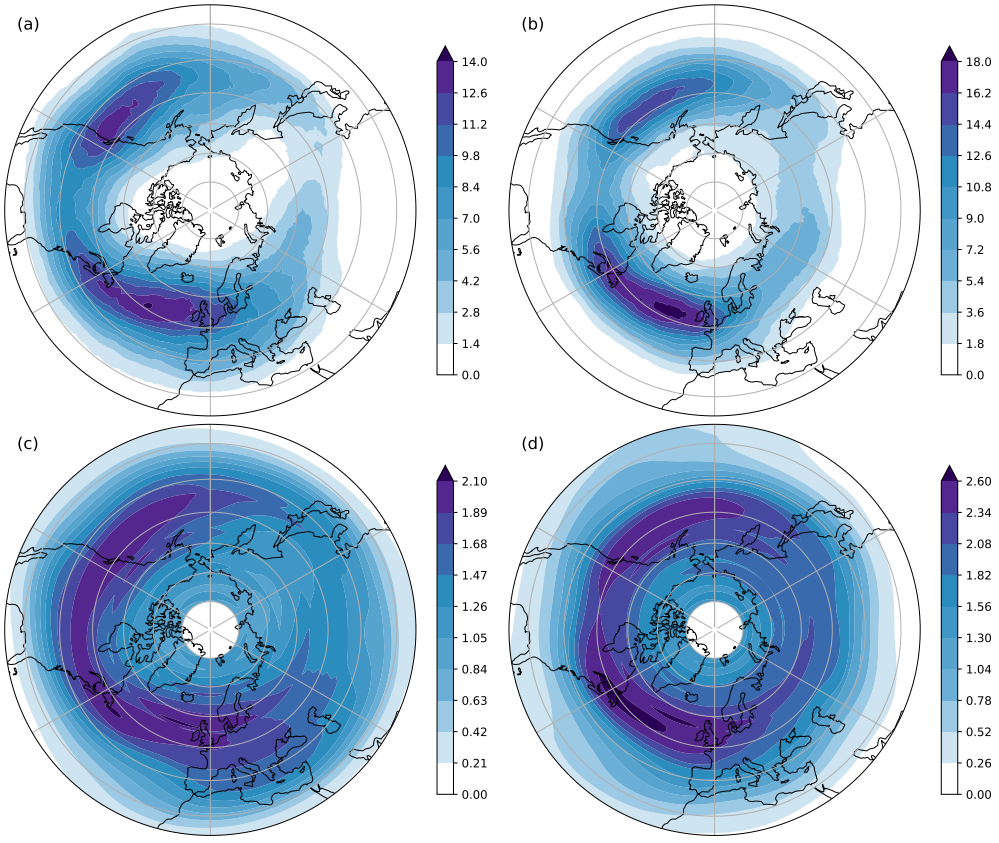

Figure 2. Occurrence frequency of RWP objects considered in this study (a) and b), in %) and the climatological mean of the RWP PV-envelope E (c) and d), in PVU, as defined by Eq. 1). Note the different scales of the color bars. Occurrence frequency is defined as the frequency of a grid point to be located within the area attributed to an RWP object. The left row (a) and c)) shows extended winter and the right row (b) and d)) shows extended summer.

2.2 Methods

2.2.1 Potential vorticity

We consider Ertel (1942) PV (q) on isentropic levels with the hydrostatic approximation $q = \sigma^{-1}(\zeta_\theta + f)$, where ζ_θ is the component of relative vorticity perpendicular to an isentropic surface, f is the Coriolis parameter, and $\sigma = -g^{-1}(\partial p/\partial\theta)$ is the isentropic layer density with gravity g, pressure p, and potential temperature θ. Our focus is on PV anomalies, q', which are defined as deviations from a climatological mean state (specifically: the daily averages of the years 1980–2019, further smoothed by a 30-day running mean). We analyze q' on isentropic levels that intersect the climatological maximum of the midlatitude PV gradient. The dynamics of RWPs is well represented by the evolution of q' on these levels, which vary through the seasons (Teubler and Riemer, 2016, 2021). Following the recommendation of Röthlisberger et al. (2018) we use

https://doi.org/10.5194/egusphere-2026-3447
Preprint. Discussion started: 29 June 2026

the following levels: 320 K for December, January, February, and March, 325 K for April and November, 330 K for May and October, 335 K for June and September, and 340 K for July and August. Interpolation from pressure levels to isentropic levels is performed using the algorithm implemented by May et al. (2022).

2.2.2 Length-scale filter and envelope computation

Using Fourier decomposition of q in the zonal direction, we filter for length scales $[L_{min}, L_{max}]$ that correspond to the wavenumber range 4–15 at 50°N, which is a typical wavenumber range used to identify RWPs (Wirth et al., 2018). We consider latitudes from 35°N–70°N. At each latitude ϕ, only wavenumbers that correspond to the length scale range $[L_{min}, L_{max}]$ are retained. The PV anomalies q'_{RWP} within this range of length scales constitute the underlying wave pattern. The envelope E (of q'_{RWP}) is computed by the (simple) Zimin et al. (2003) method:

$$E(\lambda, \phi) := 2 \left| \sum_{k=k_{min}}^{k_{max}} c_k(\phi) e^{ik\lambda} \right|, \tag{1}$$

where k_{min} and k_{max} are the (latitude-dependent) wavenumbers that correspond to L_{min} and L_{max}, $q'(\phi, \lambda) = \sum_{-\infty}^{\infty} c_k(\phi) e^{ik\lambda}$, and $c_k(\phi)$ is the Fourier coefficient of zonal wavenumber k. Importantly, only positive wavenumbers $k > 0$ are retained in the construction of E.

More refined variants to compute the envelope are usually applied for the purpose of tracking and characterizing RWP objects. The goal of these refinements is to reduce merging and splitting of RWP objects and hence to improve tracking with time and along an undulating waveguide. In the context of the current study, the refinements would impact on both, the envelope and the underlying wave pattern in a consistent manner. The benefit of more refined methods for the current study is thus not clear to us. We therefore prefer the simple and computationally much more inexpensive method by Zimin et al. (2003), which greatly facilitates the lead-time dependent comparison of re-forecasts and re-analyses over an extended time period.

For the purpose of this study, it is important that we can use E as a proxy for RWPs, i.e., characteristics of E within RWPs should be distinct from characteristics outside of RWPs. As our benchmark for the identification of RWPs we here use the RWP objects selected from Prestel-Kupferer et al.'s catalog. The climatological mean distribution of E (Fig. 2c,d) compares well with the occurrence frequency of RWP objects (Fig. 2a,b). In general, the climatological maxima of E coincide with regions of highest occurrence frequency of RWP object. One more specific difference is that the minimum over the continents is less pronounced for E than for RWP-object occurrence frequency, in particular over North America. For a more direct comparison between E and the wind-field envelope that underlies the definition of our RWP objects, E is presented in Fig. 3 for the case shown in Fig. 1. Overall, E exhibits a patchier appearance, in particular with less meridional coherence, and a more zonal orientation. These differences can be attributed to using the simple method by Zimin et al. (2003) for E, which diagnoses the wave signal in the zonal direction, whereas the wind envelope in Fig. 1 is computed diagnosing the wave signal along the streamlines of an undulating background flow. Accordingly, the specific maxima of E and of the wind envelope do not exhibit good spatial agreement. In a more general sense, however, it is clear that enhanced values of E tend to occur in regions of enhanced values of the wind envelope, i.e., within RWP objects, and that E does exhibit a reasonably high degree of spatial

https://doi.org/10.5194/egusphere-2026-3447
Preprint. Discussion started: 29 June 2026

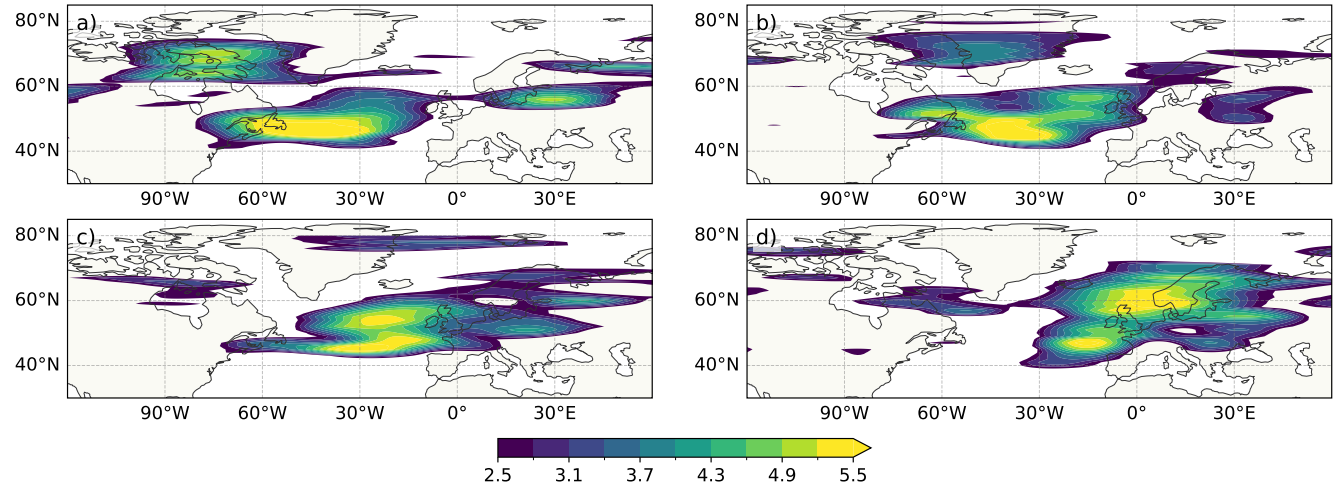

Figure 3. As Fig. 1, but for the PV envelope (in PVU) computed along latitude circles (following the 'simple' method by Zimin et al., 2003).

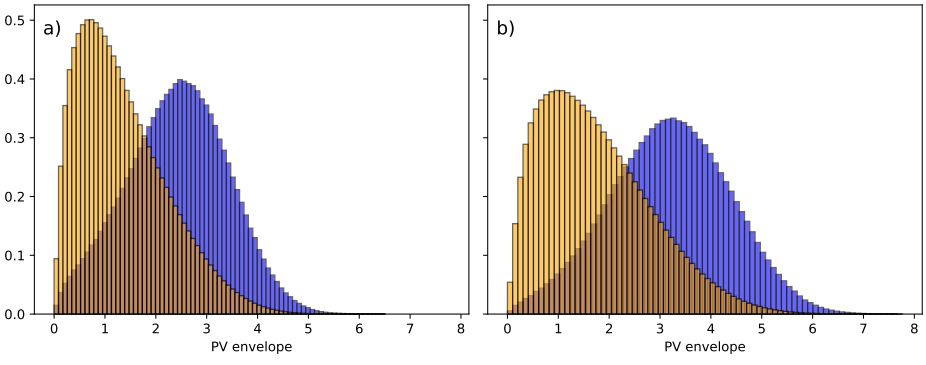

Figure 4. The distribution of envelope values E inside (blue) and outside (orange) of the RWP objects considered in this study for a) extended winter (with median values of 2.45 and 1.19, respectively) and b) extended summer (with median values of 3.21 and 1.58, respectively).

coherence. To quantify the former, we finally examine the distribution of E-values inside and outside of the RWP objects (Fig. 4). These distributions are clearly distinct, with substantially increased values of E within RWP objects. We therefore conclude that the characteristics of E (and hence q'_{RWP}) are sufficiently distinct for RWPs compared to regions outside of RWP such that E constitutes a useful metric to study RWP predictability.

https://doi.org/10.5194/egusphere-2026-3447
Preprint. Discussion started: 29 June 2026

2.2.3 Mean square error and saturation level

A forecast error Δ is defined as the difference between the forecast and the analysis. We use the mean square error (MSE) as our error metric, defined as

$$\text{MSE} := \frac{1}{A}\int_{\mathcal{A}} \Delta^2 da\,, \tag{2}$$

i.e., the spatial average of the squared error over the region $\mathcal{A}$ with area A. We will consider two regions: i) the region between 35°N–70° where the amplitude of E exceeds a specified percentile threshold (to filter low-amplitude noise) and ii) the more specific region of individual RWPs, as available from the catalog of RWP objects. Using the shorthand $\overline{(\cdot)} := \frac{1}{A}\int_{\mathcal{A}}(\cdot)da$, the MSE can be written as

$$\text{MSE} := \overline{\Delta^2} = \overline{(f-a)^2} = \overline{(f-c+c-a)^2} = \overline{(f-c)^2} + \overline{(a-c)^2} - 2\overline{(f-c)(a-c)}\,, \tag{3}$$

where f and a denote a quantity in the forecast and the analysis, respectively, and c denotes a climatological mean state computed from the analysis. For computational ease, we define this mean as the temporal mean over the same period over which we analyze errors. The first two terms on the RHS of Eq. 3 denote the variance in the forecast[1] and in the analysis, respectively. The last term denotes the covariance of deviations from climatology in the forecast and in the analysis. When this covariance vanishes, the errors saturate. The saturation level of the MSE, MSE_s, is thus given by

$$\text{MSE}_s = \overline{(f-c)^2} + \overline{(a-c)^2}\,, \tag{4}$$

i.e., by the sum of the variance of the forecast and the analysis. It is important to note that the saturation level depends on the area $\mathcal{A}$ that is used in the specification of the MSE.

The variance of our two RWP metrics, E and q'_{RWP} are shown in Fig. 5. The spatial patterns of both variances are very similar and, as can be expected, highlight the storm track regions. Note that the variance of q'_{RWP} is more than twice as large as that of E in the storm track region. Accordingly, the saturation level can be expected to be higher. We further note that the climatological mean of the PV anomalies q'_{RWP} is by definition (approximately) zero, whereas the climatological mean of E is comparable to that of the variance (cf. Fig. 2).

3 Error tendency equations and error-growth mechanisms

3.1 Piecewise PV tendencies

The PV tendency equation in isentropic coordinates reads

$$\frac{\partial q}{\partial t} = -\boldsymbol{v}\cdot\nabla_\theta q + N, \tag{5}$$

[1]The assumption that justifies this terminology is that the climatological mean of the forecast equals that of the analysis, i.e., that the forecast does not exhibit a bias. Even without this assumption, however, the term $\overline{(f-c)^2}$ serves as a metric of variability, or 'activity', in the forecast. There is a (small) low bias in Rossby wave amplitude (e.g., Doensen et al., 2024). This bias impacts similarly on both features that we compare, the underlying wave pattern (q'_{RWP}) and the Rossby wave envelope (E), and we find no indication that the bias affects the interpretation our results.

https://doi.org/10.5194/egusphere-2026-3447
Preprint. Discussion started: 29 June 2026

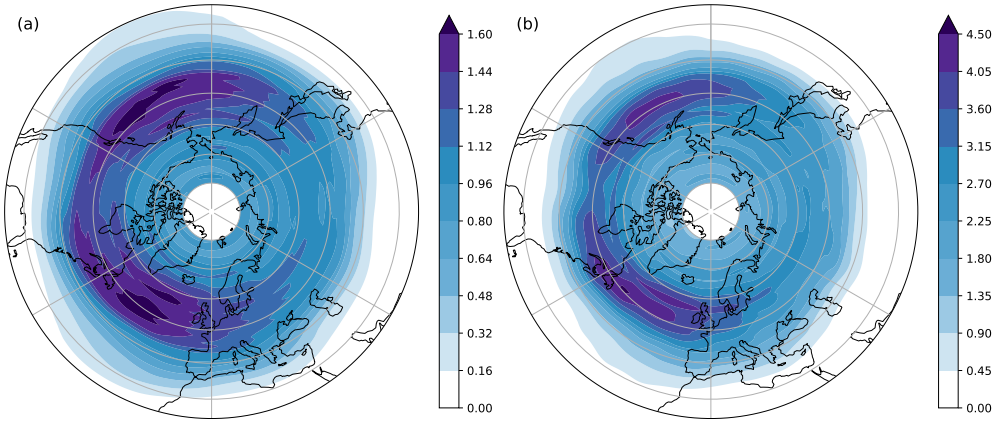

Figure 5. Variance (in PVU^2) of the PV envelope E (a)) and of the underlying wave pattern (b)), exemplified for brevity for extended summer only. Note the difference scales of the color bars. Values should be compared to the mean of the PV envelope E (Fig. 2d) and that of the underlying wave pattern, which is approx. 0. The variances for winter (not shown) look qualitatively very similar.

where $\boldsymbol{v}$ is the quasi-horizontal wind on an isentropic surface, ∇_θ is the quasi-horizontal, isentropic gradient, and N represents nonconservative processes. We here neglect N because initial condition errors in ERA5 reanalysis are of large enough amplitude that the subsequent growth of forecast errors can be expected to be dominated by advective processes (cf. Baumgart et al., 2018; Baumgart and Riemer, 2019; Selz et al., 2022). Our analysis will focus on the relative importance of these advective processes.

We decompose the advective PV tendency following standard PV thinking for midlatitude dynamics (Hoskins et al., 1985; Davis and Emanuel, 1991) and as described in some detail in appendix A of Teubler et al. (2023). The decomposition reads

$$-\boldsymbol{v}\cdot\nabla_\theta q = \mathrm{BG} + \mathrm{ADV} + \mathrm{WAVE} + \mathrm{BC} + \mathrm{DIV} + \mathrm{EDDY} + \mathrm{RES}\,, \tag{6}$$

where

$$\mathrm{BG} := -\boldsymbol{v}_0\cdot\nabla_\theta q_0 \tag{7}$$

$$\mathrm{ADV} := -\boldsymbol{v}_0\cdot\nabla_\theta q' \tag{8}$$

$$\mathrm{WAVE} := -\boldsymbol{v}_{up}\cdot\nabla_\theta q_0 \tag{9}$$

$$\mathrm{BC} := -\boldsymbol{v}_{low}\cdot\nabla_\theta q_0 \tag{10}$$

$$\mathrm{DIV} := -\boldsymbol{v}_{div}\cdot\nabla_\theta q \tag{11}$$

$$\mathrm{EDDY} := -\nabla_\theta(\boldsymbol{v}_{rot}q')\,. \tag{12}$$

The index 0 denotes climatological-mean variables (hereafter referred to as background variables) and the prime derivations thereof. A Helmholtz decomposition is applied to decompose $\boldsymbol{v}'$ into its non-divergent and ir-rotational components $\boldsymbol{v}_{rot}$ and $\boldsymbol{v}_{div}$, respectively: $\boldsymbol{v}' = \boldsymbol{v}_{rot} + \boldsymbol{v}_{div}$. Piecewise PV inversion is applied to decompose the non-divergent wind in com-

https://doi.org/10.5194/egusphere-2026-3447
Preprint. Discussion started: 29 June 2026

ponents associated with low-level ($p \geq 650$ hPa) and upper-level ($p \leq 600$ hPa) PV anomalies, $\boldsymbol{v}_{low}$ and $\boldsymbol{v}_{up}$, respectively: $\boldsymbol{v}_{rot} = \boldsymbol{v}_{low} + \boldsymbol{v}_{up}$. The piecewise PV inversion is described in detail in Teubler and Riemer (2021). The decomposition of PV tendencies in Eq. 6 has been successfully used in several previous studies (Teubler et al., 2023; Hauser et al., 2023, 2024, 2025) and is the decomposition of PV tendencies that is available for the current study. The decomposition into the six terms defined by Eqs. 7–12 is mathematically complete. The residuum term RES is introduced in Eq. 6 to represent discretization and interpolation errors and inaccuracies inherent in piecewise PV inversion. The term RES is small and does not affect the physical interpretation of our results, and is thus omitted from further analysis.

The physical interpretation of the individual terms defined by Eqs. 7–12 is as follows. The term BG represents advection of background PV by the background flow. This term is very small compared to the other terms and cancels out in the derivation of the error tendency equation below. The term ADV represents the advection of PV anomalies by the background flow. (In terms of wave dynamics, this term represents the Doppler shift.) The term WAVE represents advection of background PV by the flow associated with upper-level PV anomalies, which essentially represents the intrinsic propagation of Rossby waves along the background PV gradient. The term BC represents advection of background PV by the flow associated with low-level PV anomalies, which signifies the baroclinic coupling of the upper levels with the lower levels. This mechanism leads to baroclinic growth of the upper-level PV anomalies, i.e., amplification of upper-level troughs and ridges. The term DIV represents advection of the full PV, $q = q_0 + q'$, by the ir-rotational flow. Large values of this term are usually associated with latent heat release below, explicitly shown and further discussed in Teubler and Riemer (2021) and Hauser et al. (2023); see also Steinfeld and Pfahl (2019); Sánchez et al. (2020). It is thus sensible to interpret this term – at least in large parts – as an indirect impact of moist processes. Dominant contributions to DIV include latent heat release in warm conveyor belts in the midlatitude storm tracks and summertime continental convection. Finally, the term EDDY represents the divergence of eddy PV fluxes, i.e., the redistribution of PV by (highly) nonlinear processes.

3.2 Error tendency equations

3.2.1 PV errors

PV errors are defined as the difference between the forecast and in the analysis: $\Delta q := q_f - q_a$, where the indices f and a denote a variable in the forecast and the verifying analysis, respectively. Davies and Didone (2013) introduced the idea of a tendency equation for PV errors. A generic version of such an equation reads

$$\frac{\partial \Delta q}{\partial t} = \frac{\partial (q_f - q_a)}{\partial t} = \frac{\partial q_f}{\partial t} - \frac{\partial q_a}{\partial t} = -(\boldsymbol{v}_f \cdot \nabla_\theta q_f - \boldsymbol{v}_a \cdot \nabla_\theta q_a). \tag{13}$$

Using the individual piecewise PV tendency terms (Sect. 3) and indicating the difference between the individual terms in the forecast and in the analysis by Δ, yields

$$\frac{\partial \Delta q}{\partial t} = \Delta\text{ADV} + \Delta\text{WAVE} + \Delta\text{BC} + \Delta\text{DIV} + \Delta\text{EDDY}. \tag{14}$$

https://doi.org/10.5194/egusphere-2026-3447
Preprint. Discussion started: 29 June 2026

Note that the term BG is the same in the forecast and the analysis and thus cancels out. Introducing the positive definite (squared) error metric $\frac{1}{2}(\Delta q)^2$ (following Baumgart et al., 2018), we get

$$\frac{1}{2}\frac{\partial(\Delta q)^2}{\partial t} = \Delta q(\Delta\text{ADV} + \Delta\text{WAVE} + \Delta\text{BC} + \Delta\text{DIV} + \Delta\text{EDDY}). \tag{15}$$

In this framework, we attribute the growth of forecast errors to differences in the advection of PV anomalies, differences in the intrinsic propagation of Rossby waves, differences in baroclinic growth, differences in the impact of moist processes, and differences in the nonlinear redistribution of PV. In the case studied by Baumgart et al. (2018), error growth due to near-tropospheric dynamics (here: ΔADV + ΔWAVE + ΔEDDY) is dominated by nonlinear dynamics. It can thus be expected that the terms ΔADV and ΔWAVE here play a subordinate role relative to ΔEDDY.

3.2.2 Envelope errors

To derive a tendency equation for envelope errors, we first derive a tendency equation for the envelope itself. Expanding the definition of the envelope yields

$$E := 2\left|\sum_{k>0} c_k e^{ikx}\right| = 2\sqrt{\left(\mathcal{R}\sum_{k>0} c_k e^{ikx}\right)^2 + \left(\mathcal{I}\sum_{k>0} c_k e^{ikx}\right)^2}, \tag{16}$$

where $k = [k_{min}, k_{max}]$ and $\mathcal{R}$ and $\mathcal{I}$ denote the real and imaginary part of the sum, respectively. Using $\mathcal{R}$ and $\mathcal{I}$ as short-hand notation for these real and imaginary parts, differentiating yields

$$\frac{\partial E}{\partial t} = 2\frac{1}{2}\left(\mathcal{R}^2+\mathcal{I}^2\right)^{-1/2}\frac{\partial}{\partial t}\left(\mathcal{R}^2+\mathcal{I}^2\right) = 4\frac{\mathcal{R}\frac{\partial \mathcal{R}}{\partial t} + \mathcal{I}\frac{\partial \mathcal{I}}{\partial t}}{E}. \tag{17}$$

Noting that $c_k = c_r + ic_i$, we can write $\mathcal{R} = \frac{1}{2}\sum_{\pm k} c_k e^{ikx}$ and $\mathcal{I} = \frac{1}{2}\sum_{\pm k}(c_i + ic_r)e^{ikx}$. Denoting the Fourier coefficients of the (piecewise) PV tendencies as $c_k^t = c_r^t + ic_i^t$ we can write the tendencies $\frac{\partial \mathcal{R}}{\partial t} = \frac{1}{2}\sum_{\pm k} c_k^t e^{ikx}$ and $\frac{\partial \mathcal{I}}{\partial t} = \frac{1}{2}\sum_{\pm k}(c_i^t + ic_r^t)e^{ikx}$. We can thus evaluate the envelope tendency $\partial E/\partial t$ based on the knowledge of (the Fourier coefficients of) the PV anomalies and the PV tendencies. Being able to compute $\partial E/\partial t$ from the (piecewise) PV tendencies further implies that the decomposition into individual mechanisms introduced in Sect. 3.1 translates to the evolution of the envelope field. Formally, we may write

$$\frac{\partial E}{\partial t} = \text{BG}|_E + \text{ADV}|_E + \text{WAVE}|_E + \text{BC}|_E + \text{DIV}|_E + \text{EDDY}|_E, \tag{18}$$

where $(\cdot)|_E$ denotes the contribution of the respective mechanisms to the evolution of the envelope field. Introducing the squared error metric ΔE^2, we can write in direct analogy to the (squared) PV-error equation

$$\frac{1}{2}\frac{\partial(\Delta E)^2}{\partial t} = \Delta E(\Delta\text{ADV}|_E + \Delta\text{WAVE}|_E + \Delta\text{BC}|_E + \Delta\text{DIV}|_E + \Delta\text{EDDY}|_E). \tag{19}$$

Evaluating and comparing Eq. 19 and Eq. 15 enables us to compare the individual mechanisms that contribute to error growth of the envelope and of the underlying wave pattern.

https://doi.org/10.5194/egusphere-2026-3447
Preprint. Discussion started: 29 June 2026

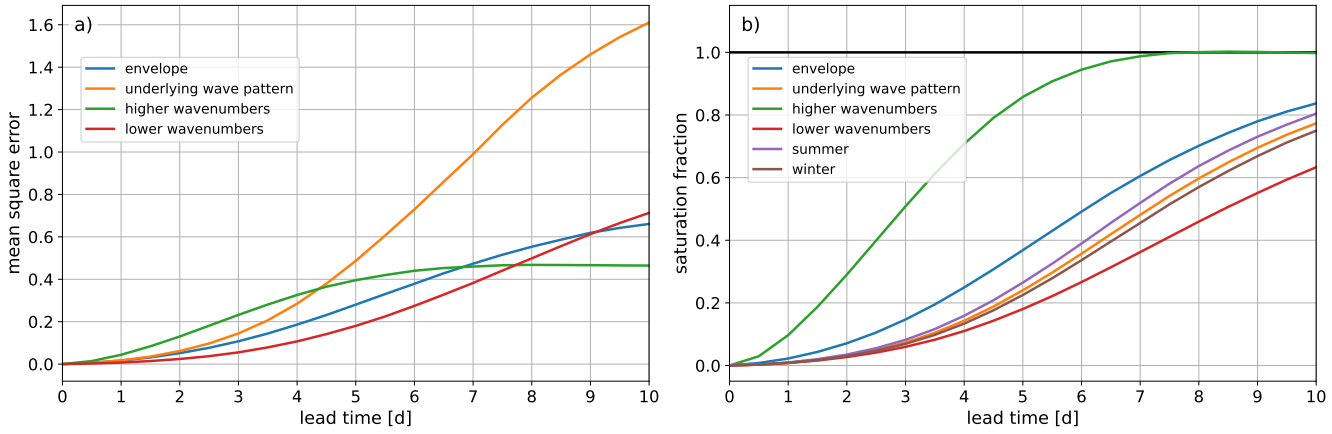

Figure 6. Error evolution within the (upper) 50th percentile of envelope values E, averaged over all months. a) absolute MSE values (in PVU) and b) saturation fraction. See the inlays for the meaning of the different colors. In b), the labels 'summer' and 'winter' refer to the underlying wave pattern averaged over extended summer and extended winter, respectively.

4 Predictability characteristics

4.1 Error growth and predictability

Figure 6a presents the absolute values of MSE, averaged year-round and over the regions in which values of the envelope exceed a certain percentile value (here, rather arbitrarily, the median). This threshold is introduced to focus the analysis on the storm tracks (cf. Fig. 2c,d). Qualitatively, there is negligible sensitivity to the choice of the threshold (not shown). The absolute MSE is shown for the envelope (blue), the PV anomalies of the underlying wave pattern (orange), and for PV anomalies of higher (green) and lower (red) wavenumbers. From the perspective of absolute MSE values, the envelope exhibits smaller errors than the underlying wave pattern. Importantly, however, this perspective does not address the question of predictability. We illustrate this important point by considering the well known scale dependence of predictability (e.g., Lorenz, 1969), i.e., the increase of predictability with scale. Seemingly consistent with this scale dependence, the absolute MSE of the higher wavenumbers exhibits the largest values initially and saturates around day 7. After day 4.5 and day 8, however, the absolute MSE values are smaller than those of the underlying wave pattern and of the lower wavenumbers, respectively. Evidently, considering the absolute values of MSE in isolation does not correctly describe the well known predictability characteristic of scale dependence.

Rather, a relevant metric for predictability is the MSE relative to the appropriate saturation level (Fig. 6b). Based on this *relative* MSE, hereafter referred to as saturation fraction, several previous studies have defined the predictability time of a feature as the lead time when a certain threshold of the saturation fraction is exceeded. The choice of this threshold is rather arbitrary. For example, Selz et al. (2022) considered thresholds of 0.8 and 0.5. Using here a threshold value of 0.6 for the mere purpose of illustration, Fig. 6b indicates predictability times of 3.5 days, 8 days, and 9.5 days for the three different wavenumber

https://doi.org/10.5194/egusphere-2026-3447
Preprint. Discussion started: 29 June 2026

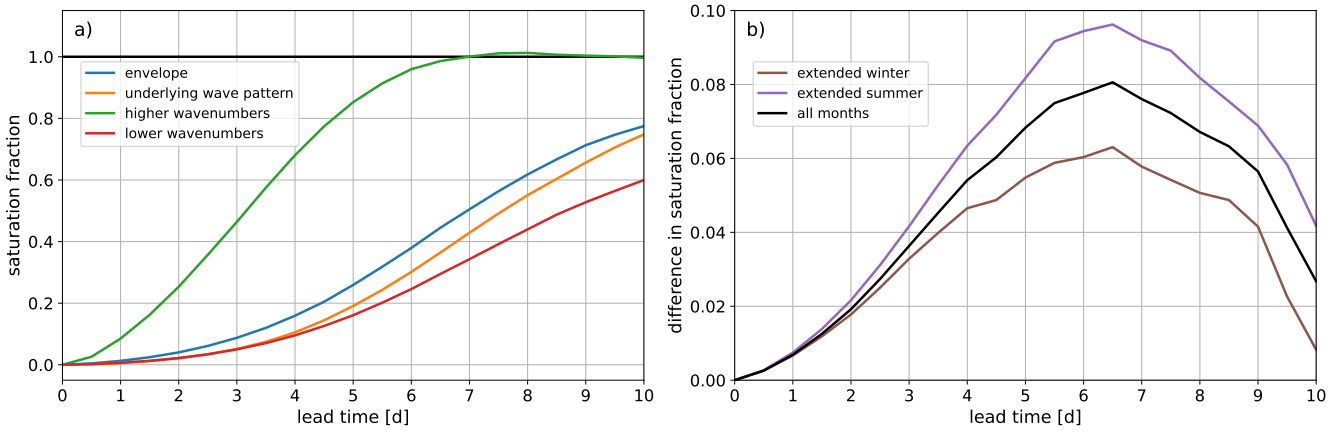

Figure 7. a) Error evolution (saturation fraction) within the RWP objects considered in this study, averaged over all months. b) Differences (in absolute terms) between the saturation fraction of the envelope and the underlying wave pattern, averaged over all months, extended winter, and extended summer, respectively. See inlays for the meaning of the different colors.

ranges, respectively, clearly revealing the scale dependence of predictability. For further illustration, Fig. 6b also demonstrates that PV anomalies (of the underlying wave pattern) exhibit a lower predictability time during summer (violet, approx. 7.6 days) than during winter (orange, approx. 8.3 days), consistent with the lower predictability of RWPs during summer found by Prestel-Kupferer et al. (2024) and lower general verification scores of operational centers during summer (e.g. Haiden et al., 2022). More generally, it can be said that, at any a given lead time, a feature exhibits higher predictability than another feature if the saturation fraction at that lead time exhibits smaller values. For example, the saturation fraction of PV anomalies with higher wavenumbers exhibits the largest values throughout. Errors in this wavenumber range fully saturate after day 7. The agreement with the saturation level at long lead times is very good, providing visual confirmation that the saturation level has been determined appropriately.

With respect to the saturation fraction of the envelope, Fig. 6 indicates substantially higher values at all lead times than for the saturation fraction of the underlying wave pattern. In the storm tracks in general, as here identified by a percentile threshold of envelope values, the hypothesis that the RWP envelope exhibits higher predictability than the underlying wave pattern has to be rejected. Rather the opposite, a higher predictability of the underlying wave pattern, seems to be the case.

The important question now is: Does this result hold if the analysis is focused specifically on RWPs, i.e., wave packets that, by definition of common RWP identification and tracking algorithms, exhibit substantial amplitude with coherent structure in both space and time? Figure 7 gives a confirmative answer. For this figure, the saturation fraction has been determined only in the regions of RWP objects, as identified and tracked by Prestel-Kupferer et al. (2024) (see Sect. 2.1.2). While the difference between the saturation fraction of the envelope and that of the underlying wave pattern is smaller than in the storm tracks in general (cf. Fig.6b), there is still no indication that the RWP envelope exhibits enhanced predictability. This result holds for both the extended winter and extended summer season, with the smallest differences in predictability found during winter

https://doi.org/10.5194/egusphere-2026-3447
Preprint. Discussion started: 29 June 2026

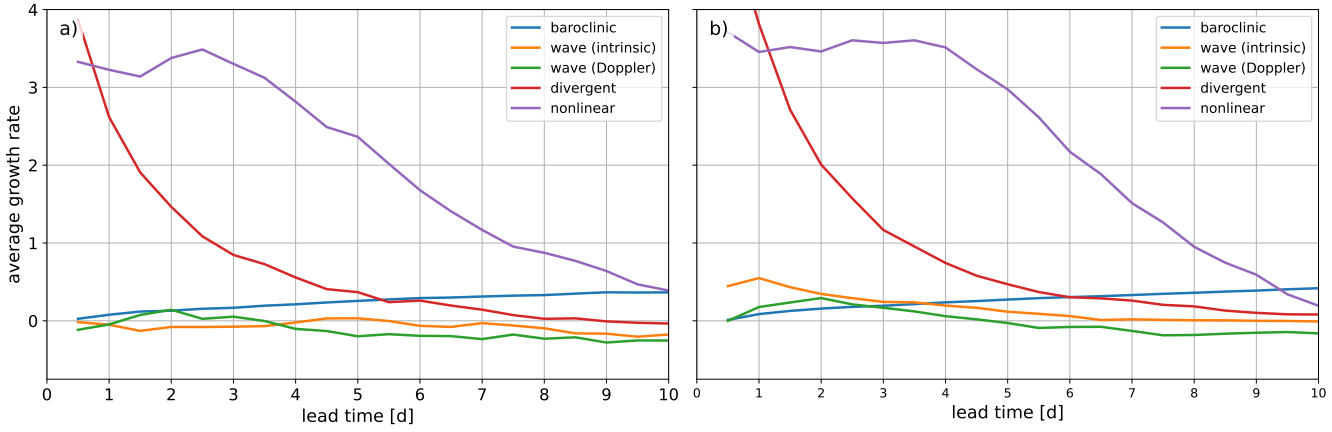

Figure 8. Mechanisms underlying error growth of the envelope E (a) and the underlying wave pattern (b) in terms of an average growth rate (in $10^{-6}\,\mathrm{m\,s^{-1}}$). The growth rate is defined by the climatological mean of the error tendencies divided by the climatological mean of the error, averaged over all months (following, e.g., Baumgart et al., 2019). See inlays for the meaning of the different colors.

(Fig. 7b). The result holds also for any region defined by a percentile threshold on the envelope field that we have considered (namely the 0^{th}, 50^{th}, 67^{th}, 75^{th}, 80^{th}, 85^{th}, 90^{th}, 95^{th}, and 98^{th} percentile). We thus reject with confidence the hypothesis that the RWP envelope exhibits higher predictability than the underlying Rossby-wave pattern.

4.2 Error-growth mechanisms

As discussed in the introduction, one plausible explanation for enhanced predictability of the wave envelope is that it removes phase information and, consequently, phase errors, which may dominate early growth of forecast errors. If this hypothesis were correct, errors in the envelope would grow primarily through mechanisms that affect wave amplitude rather than phase. Errors of the underlying wave pattern, in contrast, grow through mechanisms that impact both, amplitude and phase. The hypothesis that the wave envelope exhibits higher predictability by removing phase information thereby implies that error-growth mechanisms differ substantially between the envelope and the underlying wave pattern. In the context of the piecewise PV tendencies available to us, as described in Sect. 3.1, the terms that represent moist-baroclinic growth (BC and DIV) and wave (group) propagation (WAVE) have substantial impact on the amplitude of PV anomalies, whereas the terms that represent advection by the background flow (ADV) and the divergence of nonlinear PV fluxes (EDDY) have subordinate impacts on amplitude. A plausible expectation is thus that the terms BC, DIV, and WAVE play a more dominant role for the growth of envelope errors than for the underlying wave pattern.

Figure 8 addresses this expectation by presenting the average error-growth mechanism as a function of lead time, scaled by the average MSE at each lead time. This scaling helps to compare error-growth mechanisms over a range of error amplitudes without compromising the identification of the relative importance of different mechanisms. The striking main feature of Fig. 8 is the similarity of the mechanisms that govern error growth of the envelope and error growth of the underlying wave pattern.

https://doi.org/10.5194/egusphere-2026-3447
Preprint. Discussion started: 29 June 2026

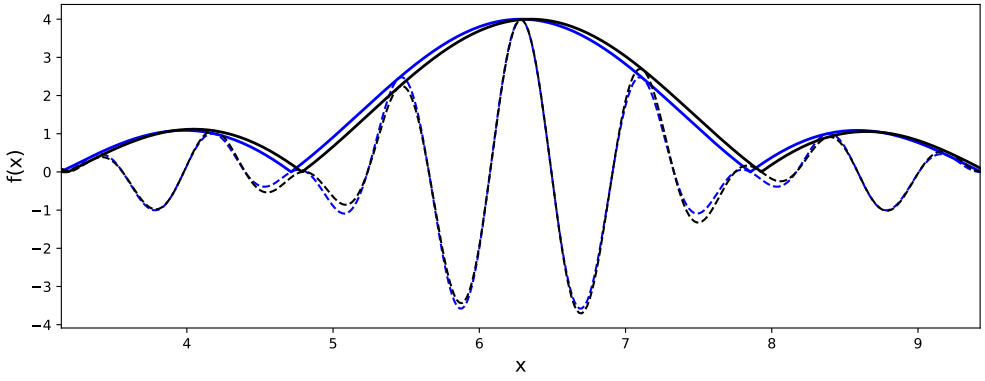

Figure 9. Synthetic wave packets consisting of wavenumbers 6–9 (dashed) and their envelope (solid). The black wave packet differs from the blue wave packet by small phase shifts of the constituent wavenumbers, specifically 0.1, 0.05, -0.05, and -0.1 for wavenumbers 6, 7, 8, and 9, respectively. Note that the sum of the phase shifts add to zero.

The EDDY term impacts the growth of envelope errors to the same extent as the growth of errors in the underlying wave pattern. In addition, there is no indication that terms that dominate amplitude evolution (BC, DIV, WAVE) are of substantially larger importance for the envelope than for the underlying wave pattern.

Figure 9 provides an explanation for the striking similarity of error-growth mechanisms. The envelope eliminates phase information in the sense that the phase of the underlying wave pattern, i.e., the location of individual troughs and ridges, cannot be inferred from the envelope. Eliminating this information, however, does not imply that the envelope is not *sensitive* to the phase of the individual wavenumbers that comprise the envelope. Figure 9 illustrates this sensitivity for a synthetic wave packet of underlying wavenumbers 6–9. Introducing small phase shifts to the individual wavenumbers, specified in the figure caption, leads to a modification of the wave pattern resulting from the superposition of these wavenumbers. In this case, although the sum of the individual phase shifts is zero, the modified wave pattern exhibits higher-amplitude troughs and ridges to the East of peak amplitude and lower-amplitude troughs and ridges to the West (compare the blue and black dashed curves in Fig. 9). Consequently, the envelope shifts to the East (compare the corresponding black and the blue envelopes in Fig. 9). The emerging ”errors”, i.e., the differences in the wave pattern and in the envelope are of comparable amplitude.

In summary, our interpretation is that ”the envelope is the wave”: Errors in the phase of the wavenumbers that comprise the envelope translate into errors of the envelope. The envelope is a direct function of its underlying wavenumbers, as is evident already from the definition of the envelope (Eq. 1). In particular, the notion is mistaken that the evolution of RWPs (as identified by their envelope) involves larger-scale dynamics than that of the underlying wavenumbers.

4.3 Rossby wave packets and atmospheric predictability

While the RWP envelope does not provide increased predictability relative to the underlying wave pattern, a further important question is if the very presence of an RWP increases predictability. This question has been addressed by Grazzini and Vitart

https://doi.org/10.5194/egusphere-2026-3447
Preprint. Discussion started: 29 June 2026

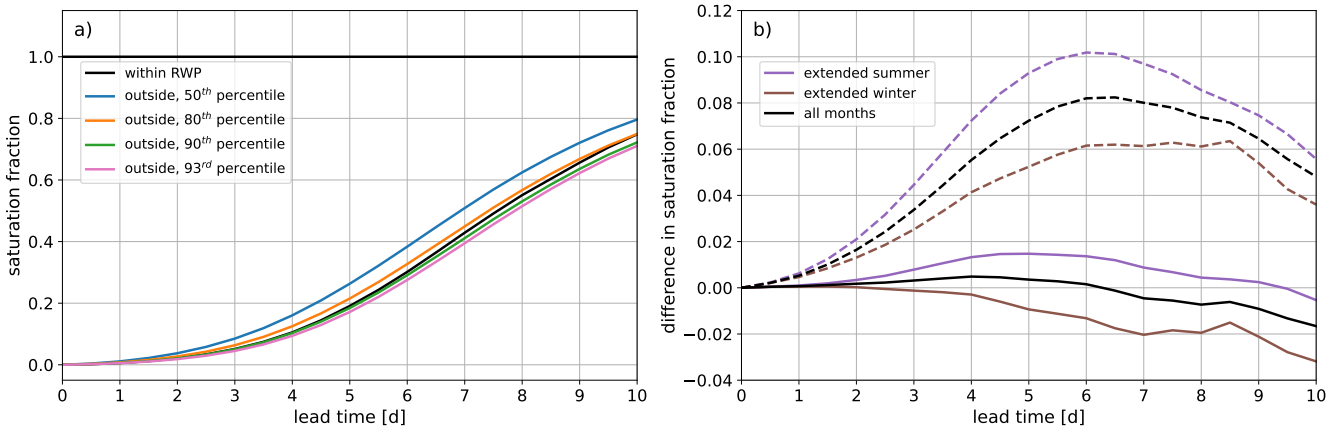

Figure 10. a) Error evolution (saturation fraction) within (black) and outside (colors) of the RWP objects, averaged over all months. The different colors denote different percentile thresholds used on the envelope field outside of RWP objects (see inlay). Note that the saturation fraction systematically decreases for higher percentile thresholds. b) Seasonal variation in the difference of the saturation fraction above the 50th outside of RWP object and within RWP objects (dashed, see inlay for the meaning of the colors) and the differences of the saturation fractions when the percentile threshold is chosen such that the PV anomalies outside and within RWP objects are on average the same (solid). Note that the differences in saturation fraction essentially vanish when controlled for the amplitude of the PV anomalies.

(2015) by investigating various skill scores of an operational forecast model over the northern hemisphere and over Europe for October–May from 2010–2012. These authors find increased predictability in the presence of RWPs, compared to situations in which RWPs are absent. We here revisit this question, considering a longer time period, a more recent operational model, and year-round predictability. Importantly, we use saturation fraction as predictability metric, whereas Grazzini and Vitart (2015) mostly present (non-normalized) MSE-type metrics. Furthermore, we focus on PV anomalies on the spatial scale of the underlying wave pattern only and shift focus from specified geographical regions to the region within RWPs. We thereby ask: Do synoptic-scale (near-tropopause) PV anomalies embedded within the envelope of an RWP object exhibit higher predictability than in average conditions?

We here define these average conditions as conditions *outside* of identified RWP objects where the envelope field still exceeds its median value. Comparing the saturation fraction of average conditions with that within RWP objects clearly indicates higher predictability within RWPs (Fig. 10a). Using (as above) an arbitrary threshold value of 0.6, the predictability time within RWPs is approx. 18 h longer, consistent with the results of Grazzini and Vitart (2015).

Figure 10a further shows, however, that predictability *outside* of RWP objects depends systematically on the value of the percentile threshold applied to the envelope field. Predictability monotonically increases when regions within higher percentiles of the envelope are considered (illustrated for the 80th, 90th, and 93rd percentile in Fig. 10a). Prestel-Kupferer et al. (2024) have found that higher-amplitude RWPs exhibit higher predictability than their lower-amplitude counterparts. Here we find that this dependence on amplitude extends to outside of the RWP objects. To control for amplitude, we select for each month a

https://doi.org/10.5194/egusphere-2026-3447
Preprint. Discussion started: 29 June 2026

percentile value for which the area-averaged amplitude of the PV anomalies outside of the RWP objects matches best with that within the RWP objects. We select from the 80th, 82nd, 84th, 86th, 88th, 89th, 90th, 91st, 92nd, and 93rd percentiles. Resulting differences in amplitude are within 1-2 % of the average for each individual month. Comparing PV anomalies within RWPs with PV anomalies that exhibit on average the same amplitude outside of RWPs, differences in predictability largely disappear for the year-round average (Fig. 10b). Because there are distinct differences between seasons, Fig. 10b presents also the results for extended summer and extended winter separately. While the predictability differences are substantially smaller for both seasons when controlling for amplitude, extended summer still exhibits higher predictability within RWPs, whereas extended winter exhibits lower predictability. We report this result here as an intriguing difference between the seasons, but leave open an interpretation of the relevance of these observed, small absolute differences for future studies. A more relevant and robust difference between the seasons is that the increase in predictability within RWPs is larger in summer than in winter if amplitude is *not* controlled for (Fig. 10b). Consistently, the amplitude of PV anomalies within RWPs correspond to that of an average percentile of 88.8 in extended summer and 85.6 in extended winter, i.e., RWPs constitute more extreme PV anomalies in extended summer than in extended winter.

Our results suggest that, to leading order, the predictability of midlatitude, synoptic-scale (PV) anomalies is controlled by their amplitude. It seems plausible that high-amplitude anomalies in general exhibit a stronger "predictive signal". The PV anomalies averaged over RWP objects are approx. within the upper 15th percentile of our data, and thus constitute substantial, high-amplitude deviations from average conditions. Within RWPs, high-amplitude anomalies are organized coherently in space and time, extending over large geographical regions for several days. It is this ability of RWPs to organize high-amplitude anomalies that is at the heart of the increased predictability that is found in the presence of RWPs.

The dynamical process underlying this organization is downstream (moist-)baroclinic development (Orlanski and Sheldon, 1995; Teubler and Riemer, 2021): Anomalies locally amplify by moist-baroclinic growth, subsequently disperse downstream by group propagation, and moist-baroclinic growth is again initiated in the downstream region. High-amplitude anomalies are thereby organized as a wave pattern along a Rossby waveguide (Manola et al., 2013; Wirth et al., 2018). While the downstream dispersion by group propagation has been stressed as a potential source of predictability since the seminal work by Cressman (1948), the state of the Rossby waveguide that would facilitate the coherent propagation of high-amplitude anomalies has received much less attention in the context of predictability. Grazzini and Vitart (2015) suggest in their concluding discussion to focus on the atmosphere's "capacity to transmit wave packets", i.e., waveguide characteristics at lead times when "the predictability of individual waves becomes very uncertain". We support their notion, but go a step further and hypothesize that waveguide characteristics impact atmospheric predictability even more directly by allowing or constraining RWP coherence in the first place.

5 Conclusions

The long-standing hypothesis has been tested that RWP envelopes are more predictable than the individual troughs and ridges that form the underlying wave pattern. To this end, we have adopted a PV perspective and used the saturation fraction of the

https://doi.org/10.5194/egusphere-2026-3447
Preprint. Discussion started: 29 June 2026

MSE as predictability metric. Deriving a tendency equation for envelope errors, the PV perspective enables the quantification of error-growth mechanisms and hence insight into predictability characteristics from an atmospheric dynamics perspective.

Very robustly, our analysis does not provide any indication of enhanced predictability of the RWP envelope. The hypothesis is therefore rejected. The error-growth mechanisms of the envelope and of the underlying wave pattern exhibit striking similarity. We demonstrate that the envelope – although it eliminates phase information in the sense that the location of individual troughs and ridges can no longer be inferred – is still *sensitive* to the phase relation of the individual wavenumbers that comprise the envelope. Phase errors in the underlying wave pattern thereby translate into envelope errors. In short, our interpretation is that "the envelope is the wave", i.e., the envelope is a direct function of its underlying wavenumbers, as one could expect from the formal definition of the envelope (Eq. 1). In particular, the notion is mistaken that RWPs (as identified by their envelope) involve larger-scale dynamics than that of the underlying wavenumbers, and that enhanced predictability may be inherited from this putative larger-scale dynamics. This erroneous notion may seem plausible when considering the RWP envelope on spatial maps (such as Fig. 1 presented herein).

We stress that still there are sensible applications of the envelope perspective in the context of predictability. In particular, because the envelope is a positive definite metric, one may extract predictive signals by averaging, e.g., over ensemble members or when time-averaged metrics are of interest, as for sub-seasonal to seasonal predictions. Averaging over the underlying wave pattern, on the other hand, the signal increasingly weakens due to the compensation between negative and positive anomalies when phase correlations between the forecast and the analysis diminish. We further note, as a limitation of our analysis, that we considered lead times up to 10 days only. While the saturation fraction of the underlying wave pattern is already large at 10-day lead time (around 0.75 - 0.8), errors are not yet fully saturated. There is indication that predictability differences diminish for high saturation fraction, and our analysis does not rule out the possibility that the RWP envelope may be indeed more predictable than the underlying wave pattern for even higher values of the saturation fraction of the underlying wave pattern.

In addition, we have revisited the important question if predictability is in general increased in the presence of RWPs. Consistent with previous work (Grazzini and Vitart, 2015), we find that predictability time is approx. 18 h longer for anomalies within RWPs than on average outside of RWPs. We furthermore find, however, that predictability of PV anomalies outside of RWPs systematically increases with increasing amplitude of the anomalies. Controlling for amplitude, i.e, comparing PV anomalies within and outside of RWPs that exhibit on average the same amplitude, predictability differences vanish. Our interpretation of this result is that it is the ability of RWPs to organize high-amplitude anomalies coherently over large geographical regions that is at the heart of the increased predictability found in the presence of RWPs. In turn, this ability to organize is facilitated by the presence of a sufficiently strong waveguide (Manola et al., 2013). Investigating the role of the Rossby waveguide for atmospheric predictability therefore emerges as a potentially fruitful topic for future studies.

Author contributions. LG performed data analysis and generated figures. MR designed the study, finalized the data analysis and figure generation, and wrote the paper.

https://doi.org/10.5194/egusphere-2026-3447
Preprint. Discussion started: 29 June 2026

Competing interests. The first author is a member of the editorial board of *Weather and Climate Dynamics*. The authors have no other competing interests to declare.

Acknowledgements. ECMWF is acknowledged for granting access to the reanalysis data. We thank Linus Magnusson (ECMWF) for facilitating the use of ERA5 re-forecast data. LG received funding from the German Research Foundation (DFG) (grant no. SFB/TRR 165, Waves to Weather).

https://doi.org/10.5194/egusphere-2026-3447
Preprint. Discussion started: 29 June 2026

References

Baldwin, M. E. and Kain, J. S.: Sensitivity of several performance measures to displacement error, bias, and event frequency, Weather and forecasting, 21, 636–648, https://doi.org/https://doi.org/10.1175/WAF933.1, 2006.

Baumgart, M. and Riemer, M.: Processes governing the amplification of ensemble spread in a medium-range forecast with large forecast uncertainty, Quarterly Journal of the Royal Meteorological Society, 145, 3252–3270, 2019.

Baumgart, M., Riemer, M., Wirth, V., Teubler, F., and Lang, S. T.: Potential vorticity dynamics of forecast errors: A quantitative case study, Monthly Weather Review, 146, 1405–1425, 2018.

Baumgart, M., Ghinassi, P., Wirth, V., Selz, T., Craig, G. C., and Riemer, M.: Quantitative view on the processes governing the upscale error growth up to the planetary scale using a stochastic convection scheme, Monthly Weather Review, 147, 1713–1731, 2019.

Cressman, G. P.: On the forecasting of long waves in the upper westerlies, Journal of Atmospheric Sciences, 5, 44–57, 1948.

Davies, H. C. and Didone, M.: Diagnosis and dynamics of forecast error growth, Monthly weather review, 141, 2483–2501, 2013.

Davis, C. A. and Emanuel, K. A.: Potential vorticity diagnostics of cyclogenesis, Monthly weather review, 119, 1929–1953, 1991.

Doensen, O., Fragkoulidis, G., Magnusson, L., Riemer, M., and Wirth, V.: Medium-range predictability of temperature extremes and biases in Rossby-wave amplitude, Quarterly Journal of the Royal Meteorological Society, 150, 5390–5402, 2024.

Ebert, E. and McBride, J.: Verification of precipitation in weather systems: Determination of systematic errors, Journal of hydrology, 239, 179–202, https://doi.org/https://doi.org/10.1016/S0022-1694(00)00343-7, 2000.

Ertel, H.: Ein neuer hydrodynamischer Erhaltungssatz, Naturwissenschaften, 30, 543–544, 1942.

Fragkoulidis, G., Wirth, V., Bossmann, P., and Fink, A. H.: Linking Northern Hemisphere temperature extremes to Rossby wave packets, Quarterly Journal of the Royal Meteorological Society, 144, 553–566, https://doi.org/https://doi.org/10.1002/qj.3228, tex.eprint: https://rmets.onlinelibrary.wiley.com/doi/pdf/10.1002/qj.3228, 2018.

Grazzini, F.: Predictability of a large-scale flow conducive to extreme precipitation over the western Alps, Meteorology and Atmospheric Physics, 95, 123–138, 2007.

Grazzini, F. and Vitart, F.: Atmospheric predictability and Rossby wave packets, Quarterly Journal of the Royal Meteorological Society, 141, 2793–2802, 2015.

Grazzini, F., Fragkoulidis, G., Teubler, F., Wirth, V., and Craig, G. C.: Extreme precipitation events over northern Italy. Part II: Dynamical precursors, Quarterly Journal of the Royal Meteorological Society, 147, 1237–1257, 2021.

Grose, W. L. and Hoskins, B. J.: On the influence of orography on large-scale atmospheric flow, Journal of Atmospheric Sciences, 36, 223–234, 1979.

Haiden, T., Janousek, M., Vitart, F., Ben-Bouallegue, Z., Ferranti, L., Prates, F., and Richardson, D.: Evaluation of ECMWF forecasts, including the 2021 upgrade, https://doi.org/10.21957/xqnu5o3p, 2022.

Hauser, S., Teubler, F., Riemer, M., Knippertz, P., and Grams, C. M.: Towards a holistic understanding of blocked regime dynamics through a combination of complementary diagnostic perspectives, Weather and Climate Dynamics, 4, 399–425, 2023.

Hauser, S., Teubler, F., Riemer, M., Knippertz, P., and Grams, C. M.: Life cycle dynamics of Greenland blocking from a potential vorticity perspective, Weather and Climate Dynamics, 5, 633–658, 2024.

Hauser, S., Teubler, F., Riemer, M., and Grams, C. M.: A quasi-Lagrangian perspective on the role of dry and moist processes in the formation of blocked North Atlantic-European weather regimes, EGUsphere, 2025, 1–31, 2025.

https://doi.org/10.5194/egusphere-2026-3447
Preprint. Discussion started: 29 June 2026

Hersbach, H., Bell, B., Berrisford, P., Hirahara, S., Horányi, A., Muñoz-Sabater, J., Nicolas, J., Peubey, C., Radu, R., Schepers, D., et al.: The ERA5 global reanalysis, Quarterly journal of the royal meteorological society, 146, 1999–2049, 2020.

Hoskins, B. J., McIntyre, M. E., and Robertson, A. W.: On the use and significance of isentropic potential vorticity maps, Quarterly Journal of the Royal Meteorological Society, 111, 877–946, 1985.

Jankov, I., Gregory, S., Ravela, S., Toth, Z., and Peña, M.: Partition of forecast error into positional and structural components, Advances in Atmospheric Sciences, 38, 1012–1019, https://doi.org/https://doi.org/10.1007/s00376-021-0251-7, 2021.

Lee, S. and Held, I. M.: Baroclinic wave packets in models and observations, Journal of Atmospheric Sciences, 50, 1413–1428, https://doi.org/https://doi.org/10.1175/1520-0469(1993)050<1413:BWPIMA>2.0.CO;2, 1993.

Lorenz, E. N.: The predictability of a flow which possesses many scales of motion, Tellus, 21, 289–307, 1969.

Manola, I., Selten, F., de Vries, H., and Hazeleger, W.: "Waveguidability" of idealized jets, Journal of Geophysical Research: Atmospheres, 118, 10–432, 2013.

Martius, O., Schwierz, C., and Davies, H. C.: Far-upstream precursors of heavy precipitation events on the Alpine south-side, Quarterly Journal of the Royal Meteorological Society, 134, 417–428, https://doi.org/https://doi.org/10.1002/qj.229, publisher: John Wiley & Sons, Ltd, 2008.

May, R. M., Goebbert, K. H., Thielen, J. E., Leeman, J. R., Camron, M. D., Bruick, Z., Bruning, E. C., Manser, R. P., Arms, S. C., and Marsh, P. T.: MetPy: A Meteorological Python Library for Data Analysis and Visualization, Bulletin of the American Meteorological Society, 103, E2273 – E2284, https://doi.org/10.1175/BAMS-D-21-0125.1, 2022.

Namias, J. and Clapp, P. F.: Studies of the motion and development of long waves in the westerlies, Journal of Atmospheric Sciences, 1, 57–77, 1944.

Orlanski, I. and Sheldon, J. P.: Stages in the energetics of baroclinic systems, Tellus A, 47, 605–628, 1995.

Pérez-Fernández, I. and Barreiro, M.: How well do forecast models represent observed long-lived Rossby wave packets during southern hemisphere summer?, Atmospheric Science Letters, p. e1175, https://doi.org/https://doi.org/10.1002/asl.1175, 2023.

Piaget, N., Froidevaux, P., Giannakaki, P., Gierth, F., Martius, O., Riemer, M., Wolf, G., and Grams, C. M.: Dynamics of a local Alpine flooding event in October 2011: moisture source and large-scale circulation, Quarterly Journal of the Royal Meteorological Society, 141, 1922–1937, https://doi.org/https://doi.org/10.1002/qj.2496, 2015.

Prestel-Kupferer, I., Riemer, M., Schmidt, S., and Teubler, F.: Predictability of midlatitude Rossby-wave packets, Quarterly Journal of the Royal Meteorological Society, 150, 5057–5073, 2024.

Quinting, J. F. and Vitart, F.: Representation of synoptic-scale Rossby wave packets and blocking in the S2S prediction project database, Geophysical Research Letters, 46, 1070–1078, https://doi.org/https://doi.org/10.1029/2018GL081381, 2019.

Röthlisberger, M., Martius, O., and Wernli, H.: Northern Hemisphere Rossby wave initiation events on the extratropical jet—A climatological analysis, Journal of Climate, 31, 743–760, 2018.

Sánchez, C., Methven, J., Gray, S., and Cullen, M.: Linking rapid forecast error growth to diabatic processes, Quarterly Journal of the Royal Meteorological Society, 146, 3548–3569, 2020.

Selz, T., Riemer, M., and Craig, G. C.: The transition from practical to intrinsic predictability of midlatitude weather, Journal of the Atmospheric Sciences, 79, 2013–2030, 2022.

Shapiro, M. A. and Thorpe, A. J.: THORPEX international science plan, WMO/TD, 1246, 2004.

Souders, M. B., Colle, B. A., and Chang, E. K.: The climatology and characteristics of Rossby wave packets using a feature-based tracking technique, Monthly Weather Review, 142, 3528–3548, https://doi.org/https://doi.org/10.1175/MWR-D-13-00371.1, 2014.

https://doi.org/10.5194/egusphere-2026-3447
Preprint. Discussion started: 29 June 2026

Steinfeld, D. and Pfahl, S.: The role of latent heating in atmospheric blocking dynamics: a global climatology, Climate Dynamics, 53, 6159–6180, 2019.

Teubler, F. and Riemer, M.: Dynamics of Rossby wave packets in a quantitative potential vorticity–potential temperature framework, Journal of the Atmospheric Sciences, 73, 1063–1081, 2016.

Teubler, F. and Riemer, M.: Potential-vorticity dynamics of troughs and ridges within Rossby wave packets during a 40-year reanalysis period, Weather and Climate Dynamics, 2, 535–559, 2021.

Teubler, F., Riemer, M., Polster, C., Grams, C. M., Hauser, S., and Wirth, V.: Similarity and variability of blocked weather-regime dynamics in the Atlantic–European region, Weather and Climate Dynamics, 4, 265–285, https://doi.org/10.5194/wcd-4-265-2023, 2023.

Wirth, V., Riemer, M., Chang, E. K., and Martius, O.: Rossby wave packets on the midlatitude waveguide—A review, Monthly Weather Review, 146, 1965–2001, 2018.

Wolf, G. and Wirth, V.: Implications of the semigeostrophic nature of Rossby waves for Rossby wave packet detection, Monthly Weather Review, 143, 26–38, 2015.

Wolf, G. and Wirth, V.: Diagnosing the horizontal propagation of rossby wave packets along the midlatitude waveguide, Monthly Weather Review, 145, 3247 – 3264, https://doi.org/https://doi.org/10.1175/MWR-D-16-0355.1, place: Boston MA, USA Publisher: American Meteorological Society, 2017.

Zimin, A. V., Szunyogh, I., Patil, D., Hunt, B. R., and Ott, E.: Extracting envelopes of Rossby wave packets, Monthly weather review, 131, 1011–1017, 2003.

Zimin, A. V., Szunyogh, I., Hunt, B. R., and Ott, E.: Extracting envelopes of nonzonally propagating Rossby wave packets, Monthly Weather Review, 134, 1329–1333, 2006.